# Quick-Response Magnetic Nanospheres for Rapid, Efficient Capture and Sensitive Detection of Circulating Tumor Cells

**Cong-Ying Wen,[†,§] Ling-Ling Wu,[†,§] Zhi-Ling Zhang,[†] Yu-Lin Liu,[‡] Shao-Zhong Wei,[‡] Jiao Hu,[†] Man Tang,[†] En-Ze Sun,[†] Yi-Ping Gong,[‡] Jing Yu,[‡] and Dai-Wen Pang[†,*]**

[†]Key Laboratory of Analytical Chemistry for Biology and Medicine (Ministry of Education), College of Chemistry and Molecular Sciences, State Key Laboratory of Virology, and Wuhan Institute of Biotechnology, Wuhan University, Wuhan 430072, People's Republic of China, and [‡]Hubei Cancer Hospital, Wuhan, 430079, People's Republic of China. [§]C.-Y. Wen and L.-L. Wu contributed equally to this work.

**ABSTRACT** The study on circulating tumor cells (CTCs) has great significance for cancer prognosis, treatment monitoring, and metastasis diagnosis, in which isolation and enrichment of CTCs are key steps due to their extremely low concentration in peripheral blood. Herein, magnetic nanospheres (MNs) were fabricated by a convenient and highly controllable layer-by-layer assembly method. The MNs were nanosized with fast magnetic response, and nearly all of the MNs could be captured by 1 min attraction with a commercial magnetic scaffold. In addition, the MNs were very stable without aggregation or precipitation in whole blood and could be re-collected nearly at 100% in a monodisperse state. Modified with anti-epithelial-cell-adhesion-molecule (EpCAM) antibody, the obtained immunomagnetic nanospheres (IMNs) successfully captured extremely rare tumor cells in whole blood with an efficiency of more than 94% *via* only a 5 min incubation. Moreover, the isolated cells remained viable at 90.5 ± 1.2%, and they could be directly used for culture, reverse transcription—polymerase chain reaction (RT-PCR), and immunocytochemistry (ICC) identification. ICC identification and enumeration of the tumor cells in the same blood samples showed high sensitivity and good reproducibility. Furthermore, the IMNs were successfully applied to the isolation and detection of CTCs in cancer patient peripheral blood samples, and even one CTC in the whole blood sample was able to be detected, which suggested they would be a promising tool for CTC enrichment and detection.

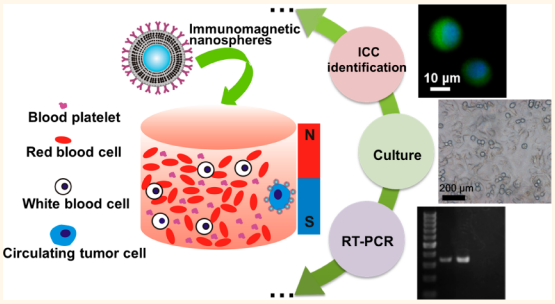


**KEYWORDS:** magnetic nanospheres · circulating tumor cells · rapid and efficient capture · sensitive detection

Carcinoma, defined as a tumor of epithelial tissue, is one of the biggest threats to human life, and most deaths from this kind of tumor are caused by metastases.[1,2] Recent researches have suggested that circulating tumor cells (CTCs), which are shed from tumor into the bloodstream, play an important role in metastases, and their level is significantly associated with prognosis and survival of patients with major cancers (breast, prostate, and colon cancer).[3,4] Therefore, CTC detection and enumeration may be used for treatment progress monitoring, cancer prognosis, and early diagnosis of metastases.[5,6] However, CTCs are extremely rare in an extremely complex matrix, that is, only up to hundreds of CTCs out of $>10^9$ hematological cells in 1 mL of blood.[7,8] Thus, highly efficient isolation and enrichment of CTCs are necessary steps in CTC-based analysis.[4,9]

In recent years, numerous approaches have been developed for CTC isolation and enrichment. They are mainly divided into two groups: those based on physical attributes, such as size,[10,11] density,[12,13] deformability,[14] and adhesion preference,[15,16] and those based on affinity, such as antibody—antigen,[8,17−20] E-selectin,[21,22] and aptamer.[23,24] Despite that each technique has its own limitation because of the heterogeneity of tumor cells, they all have achieved good enrichment effects under certain conditions.[4] Among them, magnetic separation is a widely applied and very promising tool for

* Address correspondence to dwpang@whu.edu.cn.

Received for review November 5, 2013 and accepted December 6, 2013.

**Published online December 06, 2013**
**10.1021/nn405744f**

CTC enrichment, due to its easy manipulation, high capture efficiency, and convenient coupling with identification methods such as immunocytochemistry (ICC) and polymerase chain reaction (PCR) assays.[7,20,24−33] An automated immunomagnetic enrichment for CTCs has been approved by the U.S. Food and Drug Administration (FDA) and come into the market, known as CellSearch.[4] CTC detection by CellSearch has shown high accuracy and sensitivity with good reproducibility.[7,30]

So far, both micrometer-sized magnetic beads and magnetic nanoparticles have been used in cell isolation, and they have their own advantages and disadvantages. Magnetic microbeads are used more widely due to their fast magnetic response and low loss rate during the treatment process,[20,28,29,31−33] while the magnetic nanoparticles' response is not fast enough, and they suffer higher loss rate and need a strong magnetic separation tool, making their application limited. Despite all of the above, trials to use magnetic nanoparticles continue, because they have unique advantages compared with the microbeads.[24,26,27] The nanoparticles have a relatively high surface to volume ratio, causing higher binding capacity and higher capture efficiency; their faster binding kinetics enables fast enrichment; they are stable in a matrix without aggregation or precipitation; the cells captured by them can be directly used for further analyses without a release process.[27,34−36] Thus, it will be very significant to develop a kind of nanosized magnetic bead with fast magnetic response combining the advantages of both microbeads and nanoparticles. The CellSearch system has found a method to reach this combination. As the introduction to the CellSearch system describes,[37] immunomagnetic nanoparticles (120−200 nm) modified with anti-epithelial-cell-adhesion-molecule (EpCAM) antibody and biotin analogue are first used to capture CTCs. Second, streptavidin is added to bind the biotin analogue. Third, excess immunomagnetic nanoparticles are added to bind to the bound streptavidin to amplify the volume of magnetic nanoparticles. As a result, fast magnetic response is achieved, which greatly benefits the separation process. After magnetic separation, biotin is added to competitively bind streptavidin to release excess immunomagnetic nanoparticles. However, this method introduces more steps and makes the enrichment process more complicated.

In our previous work, we constructed fluorescent-magnetic nanospheres by directly coembedding hydrophobic quantum dots (QDs) and nano-$\gamma$-$Fe_2O_3$ into poly(styrene/acrylamide) copolymer nanospheres (Pst-AAm-COOH), which had been successfully used to capture and detect cancer cells, bacteria, and proteins.[36,38−42] However, this method had some limitations in controllability and capacity to load nanoparticles due to the randomness of the embedding process and the limited space inside the nanospheres. While the layer-by-layer (LBL) assembly method has the advantage of high controllability,[43−46] we further developed an LBL assembly approach to fabricate fluorescent-magnetic dual-encoded nanospheres.[47] Quick-response magnetic nanospheres (MNs) were accordingly prepared with the LBL assembly method and used to rapidly and efficiently capture CTCs. By simply controlling the coating layers of magnetic nanoparticles, the magnetic response as well as the size of MNs could be tuned simultaneously, and finally five layers were chosen to obtain quick-response MNs with a small size, a compromise between response and size and a combination of both advantages. The MNs with a diameter of ca. 380 nm had a high magnetic saturation value of 34.9 emu/g, and nearly all of the MNs could be captured by 1 min attraction with a commercial magnetic scaffold. In addition, the MNs were very stable and did not aggregate or precipitate in the complex matrix during incubation and could be re-collected in a monodisperse state nearly at 100% in whole blood. With these unique characteristics, the MNs were modified with anti-EpCAM antibody, and the obtained immunomagnetic nanospheres (IMNs) were successfully used to capture extremely rare tumor cells in whole blood with an efficiency of more than 94% *via* a 5 min incubation. The isolated cells could be directly used for culture, RT-PCR, and ICC identification without disassociating the IMNs. ICC identification and enumeration of the tumor cells in the same blood samples showed high sensitivity and good reproducibility. Moreover, IMNs were successfully applied to cancer patient peripheral blood samples, showing their potential application in practice.

## RESULTS AND DISCUSSION

**Characterization of the IMNs.** Pst-AAm-COOH were used as templates for the construction of MNs with an LBL assembly method.[47] As Scheme 1 illustrates, on the basis of PEI layers, the hydrophobic nano-$\gamma$-$Fe_2O_3$ magnetic particles were assembled on the surface of the nanospheres through coordination between primary amines of PEI and metallic atoms from nano-$\gamma$-$Fe_2O_3$. To get a rapid magnetic response, five layers of nano-$\gamma$-$Fe_2O_3$ were assembled, and an outer layer of silica was introduced to increase the stability of the MNs. Through further modification with succinic anhydride, the MNs were equipped with carboxyl groups for further coupling with biomolecules. The TEM image (Figure 1A) demonstrated that the MNs were well dispersed without aggregation and showed good uniformity in size (376 $\pm$ 17 nm). The hydrodynamic diameter and the polydispersity index (PDI) of the MNs (Figure 1B) changed little with increasing storage time, which confirmed that the MNs retained good monodispersibility and stability for at least six months. From the magnetic hysteresis loop (Figure 1C), it can be seen that the MNs had excellent superparamagnetic

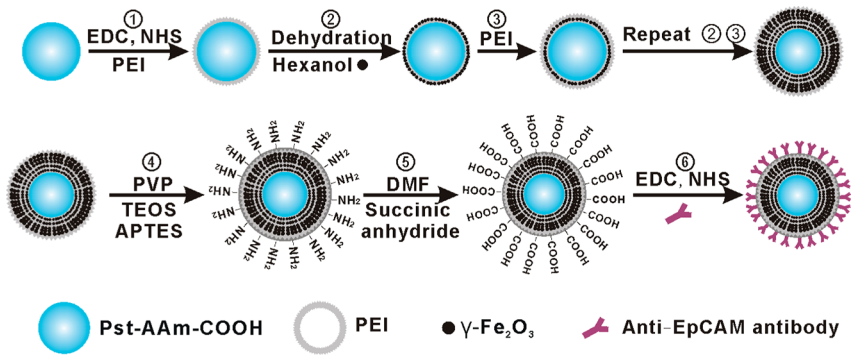


**Scheme 1. Schematic diagram for the construction of immunomagnetic nanospheres.**

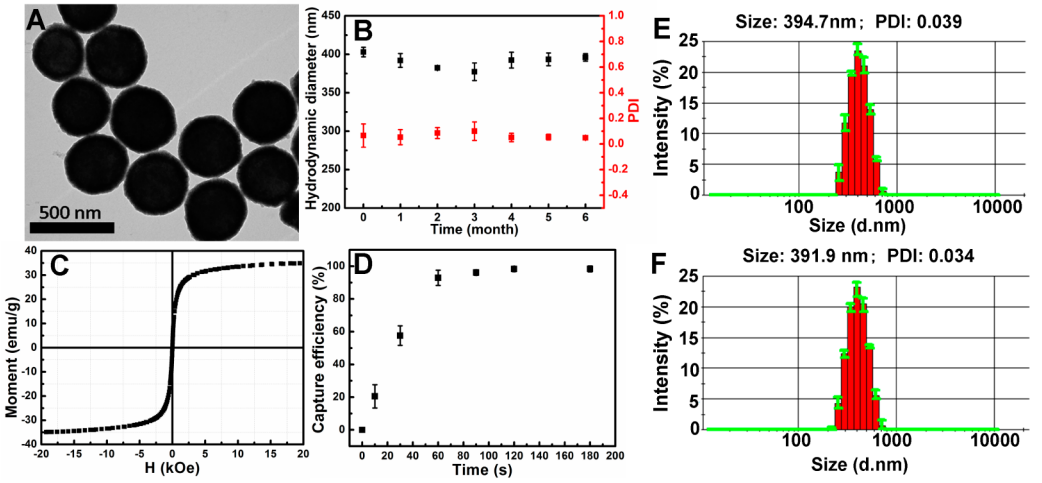


**Figure 1. Characterization of the MNs. (A) TEM image of the MNs. (B) Hydrodynamic diameters and PDI of the MNs at different storage times. (C) Magnetic hysteresis loop of the MNs measured at room temperature. (D) Capture efficiencies of MNs at different attraction times with a commercial magnetic scaffold. (E) Hydrodynamic size of the MNs. (F) Hydrodynamic size of the MNs after incubation in whole blood.**

property at room temperature with a large magnetic saturation value (34.9 emu/g), which refers to the magnetic moment per gram of MNs when the magnetization of the MNs cannot increase with increasing strength of the external magnetic field. Nearly all of the MNs could be captured by 1 min attraction with a commercial magnetic scaffold (Invitrogen, 12320D, the field strength on the surface of the magnetic scaffold was 325 ± 25 mT) (Figure 1D). The magnetic separation rates of nanospheres with different layers of nano-$\gamma$-$Fe_2O_3$ were also studied, as shown in Figure S2 (Supporting Information). The magnetic nanospheres responded faster with increasing coating layer, up to five layers; then the magnetic response increased little. Thus, five layers of nano-$\gamma$-$Fe_2O_3$ were chosen under our experimental conditions, which could ensure the manipulation was easy and quick and reduce MN loss during sample handling. Then we investigated the stability of the MNs in whole blood. The hydrodynamic size (Figure 1E and F) accurately demonstrated the stability of the MNs in a complex whole blood system, which remained almost unchanged at 391.9 nm (PDI: 0.034) after incubation compared with 394.7 nm (PDI: 0.039) before incubation. Besides, the MNs were re-collected from whole blood, and the recovery reached 98.4 ± 5.6% (S.2, Supporting Information). With all these unique characteristics, the MNs were modified with anti-EpCAM antibody, which was subsequently confirmed by the fact that the obtained IMNs could specifically interact with FITC-labeled goat anti-mouse IgG (S.3, Supporting Information). The number of active affinity sites on each IMN was evaluated to be about 100 by taking goat anti-rabbit IgG as a model antibody (S.4, Supporting Information). These all indicated that antibody was successfully conjugated to MNs and preserved its bioactivity during the coupling process. Furthermore, the stability of IMNs was also studied (S.5, Supporting Information). From Figure S5A, it can be seen that IMNs could capture more than 95% of Hep G2 cells even after 4 months' storage, which indicated that IMNs preserved their bioactivity over a long period of storage time. Additionally, dynamic light scattering (DLS) characterization (Figure S5B and C) also showed that the hydrodynamic size of IMNs changed little with increasing storage time, giving 404.8 nm (PDI: 0.219) after four months' storage

(Figure S5C) compared with 405.7 nm (PDI: 0.215) for newly prepared IMNs (Figure S5B). These results confirmed the stability of the IMNs.

**Capability of IMNs to Capture Tumor Cells.** The IMN concentration used in the capture was optimized, and the specificity for IMNs to capture tumor cells was investigated. The results are shown in Figure 2. With the increase of IMN concentration, the capture efficiency increased until the concentration reached 0.3 mg/mL, at which 96% of SK-BR-3 cells were captured (Figure 2A), while at this concentration, IMNs hardly captured any Jurkat T cells, which are a kind of human peripheral blood leukemia T cells taken as a control, and unmodified MNs could hardly capture SK-BR-3 cells either (Figure 2B), indicating that the binding between IMNs and SK-BR-3 cells was effective and specific. Immunomagnetic fluorescent nanospheres were also used to treat SK-BR-3 cells and Jurkat T cells. As Figure S6 (S.6, Supporting Information) shows, many red fluorescent immunonanospheres bound to the SK-BR-3 cell surface (Figure S6A–C), while no cell was observed in the Jurkat T cell control group (Figure S6D–F), which further confirmed the successful and specific binding between immunonanospheres and SK-BR-3 cells.

Then, the capability of IMNs to capture rare tumor cells in synthetic CTC samples was investigated. The samples were prepared by spiking stained SK-BR-3 cells into whole blood with concentrations of about 5–300 cells mL$^{-1}$. For comparison, capture efficiencies were also examined in PBS, mixed cell samples, and lysed blood spiked with similar concentrations of SK-BR-3 cells. The results are shown in Figure 3A. Regression analysis of captured cell number *versus* spiked cell number obtained $y = 0.85x$ ($R^2 = 0.997$), $y = 0.94x$ ($R^2 = 0.995$), $y = 0.90x$ ($R^2 = 0.996$), and $y = 0.89x$ ($R^2 = 1.000$) respectively in PBS, mixed cell suspension, lysed blood, and whole blood. It can be seen that IMNs could efficiently capture SK-BR-3 cells in all cases. The capture efficiencies in the four types of samples were comparable and did not have significant differences at the 0.05 level (0.95 confidence level). This suggested that complex conditions had negligible effects on the binding between IMNs and the target cells, and IMNs were able to be directly used in whole blood.

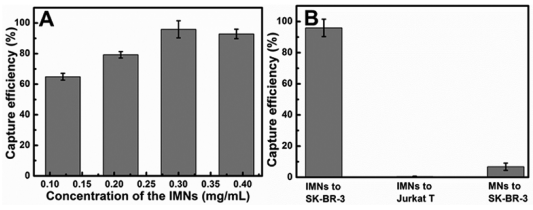


**Figure 2. Efficiencies to capture SK-BR-3 cells with different concentrations of IMNs (A) and capture efficiencies of IMNs to SK-BR-3 cells, IMNs to Jurkat T cells, and MNs to SK-BR-3 cells.**

Assay time has always been a very important factor for detection. So we investigated the efficiency to capture rare SK-BR-3 cells (*ca.* 100 cells mL$^{-1}$) in whole blood for different durations of incubation. As Figure 3B showed, 5 min incubation enabled IMNs to capture more than 94% of SK-BR-3 cells in whole blood. This indicated that IMNs had fast binding kinetics most probably due to the small size of the IMNs.[27,41] Thus, a five-minute incubation was sufficient for IMNs to bind the target cells, which can save much time for CTC detection.

Moreover, three other kinds of EpCAM-positive tumor cells were spiked in whole blood (100 cells mL$^{-1}$) and then were captured by IMNs (Figure 3C). The capture efficiencies all reached more than 92%, showing that IMNs had general applicability.

From all these experimental results, it could be concluded that IMNs were able to capture rare tumor cells from whole blood efficiently, specifically, and quickly, establishing a sound basis for CTC detection.

**ICC Identification of the Captured Cells.** Mimic clinical samples were prepared by spiking SK-BR-3 cells into healthy human blood at 50 cells mL$^{-1}$, from which tumor cells were captured with IMNs and identified with a commonly used three-color ICC method including FITC-labeled anti-cytokeratin 19 (CK19), a marker for epithelial cells, allophycocyanin (APC)-labeled anti-CD45 (CD45, a marker for white blood cells (WBCs)), and DAPI nuclear staining. Combined information was utilized to discriminate tumor cells from WBCs. Cells that had round to oval morphology were positive for DAPI and CK19 and negative for CD45 were identified as tumor cells.[8,17,18] As shown in Figure 4, cells that

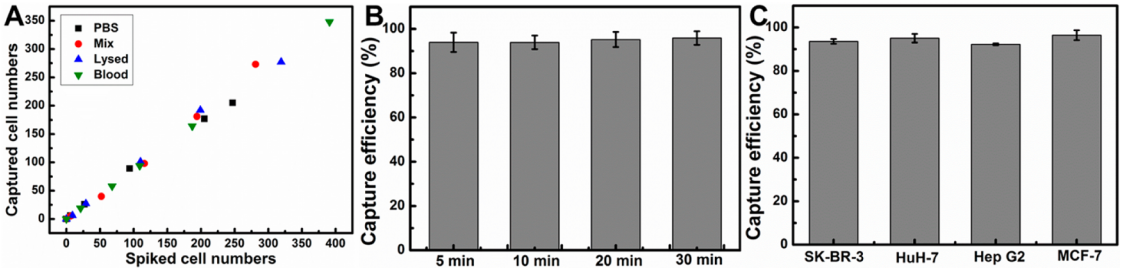


**Figure 3. (A) Capture efficiencies with IMNs at different cell concentrations (5–300 cells mL$^{-1}$) in four different types of samples: PBS (■), mixture of SK-BR-3 and Jurkat T cells (●), lysed blood (▲), and whole blood (▼). (B) Efficiencies to capture SK-BR-3 cells (*ca.* 100 cells mL$^{-1}$) in whole blood at different incubation times. (C) Capture efficiencies from whole blood spiked with four different types of tumor cells: SK-BR-3, HuH-7, Hep G2, and MCF-7 cells (tumor cell concentration: *ca.* 100 cells mL$^{-1}$).**

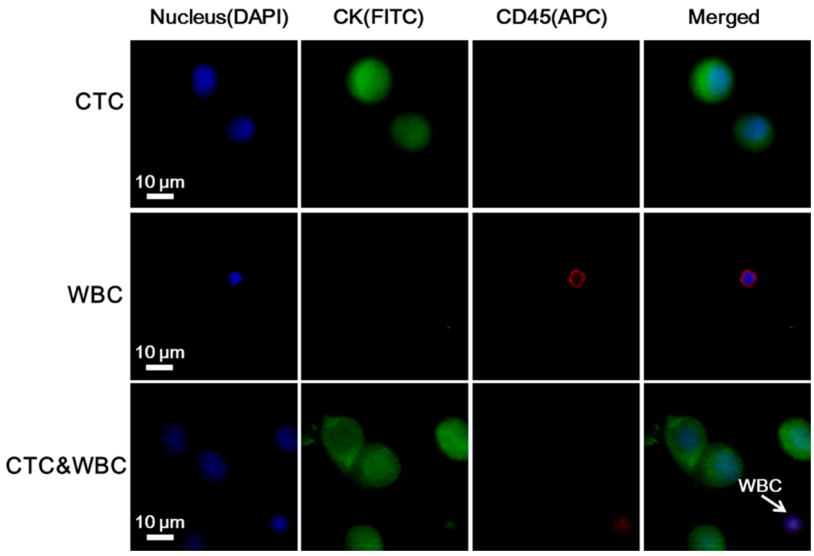


**Figure 4. Confocal microscopic images of cells captured from mimic clinical blood samples and identified with the three-color ICC. Nucleus (DAPI): excitation 405 nm, emission 447 ± 30 nm band-pass. CK (FITC): excitation 488 nm, emission 525 ± 25 nm band-pass. CD45 (APC): excitation 605 nm, emission 685 ± 20 nm band-pass. Merged: merge of nucleus (DAPI), CK (FITC), and CD45 (APC).**

**TABLE 1. Enumeration of Tumor Cells in Five Blood Samples**

| | measurement no. | | | | |
|---|---|---|---|---|---|
| sample no. | 1 | 2 | 3 | mean | RSD[a] |
| 1 | 7 | 6 | 6 | 6 | 9.1% |
| 2 | 29 | 29 | 35 | 31 | 11.2% |
| 3 | 13 | 12 | 16 | 14 | 15.2% |
| 4 | 21 | 19 | 19 | 20 | 5.9% |
| 5 | 20 | 22 | 17 | 20 | 12.8% |

[a] Mean RSD: 10.8 ± 3.6%.

exhibited strong CK19 expression and negligible CD45 signals were tumor cells, while cells that presented high CD45 and low CK19 expression levels were WBCs. Some hematologic cells would be nonspecifically trapped due to their very large number in blood (red blood cells (RBCs), $(3-9) \times 10^9$ cells per mL; WBCs, $(0.3-1) \times 10^7$ cells per mL),[27] which happened with all current CTC separation methods, and that was why ICC identification was necessary for CTC detection. Furthermore, the reproducibility and reliability of this method were investigated. Five groups of mimic clinical samples were examined three times respectively, and the captured tumor cells were identified and enumerated, which are shown in Table 1. The relative standard deviation (RSD) was calculated to be 10.8% compared with 18% of the commercialized CellSearch system, which confirmed the good reproducibility and reliability of this method.

**Cell Viability and RT-PCR Analyses.** Calcein AM and propidium iodide (PI) were used to stain the isolated tumor cells to analyze their viability. Calcein AM can penetrate the live cell membrane and react with the intracellular esterase to form calcein with green fluorescence, while PI is a membrane-impermeable nuclear stain that can stain only dead cells, resulting in red fluorescence.[17,19,23] From Figure 5A, it can be seen that the majority of the isolated cells showed green fluorescence, and the viability rate was calculated to be 90.5 ± 1.2%, which indicated that most of the tumor cells remained viable after the isolation. Then, we investigated whether the isolated cancer cells can be directly cultured and propagated *in vitro*. As shown in Figure 5B–E, the cells adhered well, proliferated on the culture dish, and had successfully undergone multiple (>5) passages without detectable changes in morphology and behavior. Furthermore, to determine whether the isolated cells can be directly used for molecular biological analyses, RT-PCR was used to amplify two tumor-specific mRNA, CK19 and epidermal growth factor receptor (EGFR) mRNA, which are usually used in CTC detection.[9,48] From Figure 5F and G, it can be seen that the 346-bp fragments of the CK19 coding region and 285-bp fragments of the EGFR coding region were found with the cells captured by IMNs (lane 3 in Figure 5F and G), while no fragment was found when MNs were used to treat tumor cells (lane 4 in Figure 5F and G). These suggested IMN binding had a negligible influence on RNA extraction and RT-PCR, and the captured cells can be analyzed by RT-PCR without disassociating IMNs. Also, this further confirmed the specific binding between IMNs and tumor cells. Overall, the tumor cells captured with IMNs were suitable for subsequent cell culture and molecular biological analyses, which was crucial for further research.

**Detection of CTCs in Cancer Patient Peripheral Blood Samples.** Having proved that the tumor cells could be captured with IMNs efficiently, rapidly, and specifically and detected with ICC reproducibly and reliably, we applied

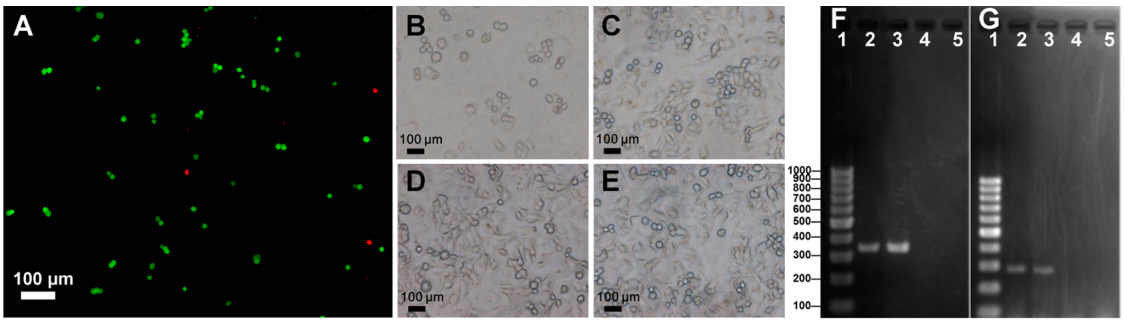


**Figure 5. Viability and RT-PCR analyses of the isolated tumor cells. (A) Fluorescence microscopic image of the captured cells stained with calcein AM (green) and PI (red). (B–E) Microscopic images of the captured tumor cells that were just attached to the flask wall (B), reached confluence (C), reached confluence after one passage (D), and reached confluence after five passages (E). (F, G) Agarose gel electrophoresis of the products from RT-PCR amplification of CK19 mRNA (F) and EGFR mRNA (G). (Lane 1, 1 kbp DNA ladder; lane 2, positive control of SK-BR-3 cells; lane 3, SK-BR-3 cells captured with IMNs; lane 4, SK-BR-3 cells treated with MNs; lane 5, negative control with sterile water as template.)**

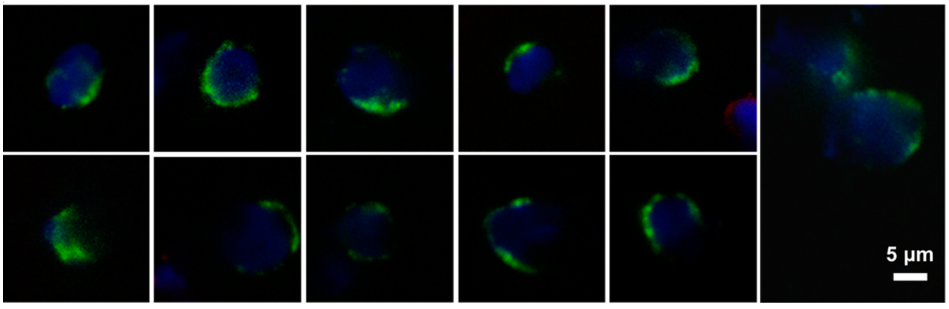


**Figure 6. Images of 12 CTCs captured with our method from 1.2 mL of blood of patient #6.**

IMNs to the detection of CTCs in the whole blood samples from 19 cancer patients (including colon, liver, lung, and breast cancer patients) and 16 healthy people. The isolated cells were also identified with the three-color ICC as described above, and cells positive for CK19 and DAPI and negative for CD45 were enumerated as CTCs. The results are summarized in Tables S1 and S2 (S.7, Supporting Information), and the images of 12 CTCs captured with our method from 1.2 mL of blood of patient #6 are shown in Figure 6. CTCs in the blood of the 19 cancer patients could be captured and detected, while no CTC was found in any healthy samples, which suggested IMNs were successfully applied to real patient blood samples, and they might be a promising enrichment tool for CTC detection.

## CONCLUSIONS

In summary, we have successfully used quick-response magnetic nanospheres for rapid, efficient capture and sensitive detection of CTCs. The MNs were fabricated by a convenient and highly controllable LBL assembly method, and they were very stable and easy to manipulate in a complex matrix. Furthermore, the MNs were nanosized with a fast magnetic response, which successfully combined the advantages of magnetic microbeads and magnetic nanoparticles in cell isolation. Modified with anti-EpCAM antibody, IMNs successfully captured more than 94% of rare SK-BR-3 cells in whole blood *via* only a 5 min incubation. The isolated tumor cells were identified and enumerated by ICC with an RSD of 10.8%, showing good reproducibility and reliability. Moreover, the IMN binding had an insignificant influence on the viability of the isolated cells, and they could be directly used for culture and RT-PCR analyses without disassociating IMNs. The IMNs were successfully employed for detecting cancer patient peripheral blood samples, validating their great application potential in CTC studies.

## MATERIALS AND METHODS

**Reagents and Instruments.** Branched poly(ethylene imine) (PEI, MW 25 kDa and MW 750 kDa), tetraethyl orthosilicate (TEOS), (3-aminopropyl)triethoxysilane (APTES), polyvinylpyrrolidone (PVP-k30), *N*-(3-dimethylaminopropyl)-*N*′-ethylcarbodiimide hydrochloride (EDC), *N*-hydroxysuccinimide (NHS), 4,6-diamidino-2-phenylindole (DAPI), bovine serum albumin (BSA), and anti-EpCAM monoclonal antibody were purchased from Sigma-Aldrich. FITC-labeled anti-CK19 monoclonal antibody and APC-labeled anti-CD45 monoclonal antibody were obtained from Abcam. The primers for PCR and Hoechst 33342 were bought from Invitrogen Corp. 2×Tag PCR master mix and RNAprep Pure Cell/Bacteria kit were purchased from Tiangen Biotech (Beijing) Co., Ltd. The reverse transcription system was obtained from Promega Corporation. Breast cancer SK-BR-3 and MCF-7 cells, liver cancer HuH-7 and Hep G2 cells, and Jurkat T cells were purchased from

China Center for Type Culture Collection. Human blood samples were supplied by Hubei Cancer Hospital. All the media for cell culture were bought from Gibco Corp. Ultrapure water (18 MΩ·cm) was made by a Millipore Milli-Q system. Fluorescence images were recorded with a CCD camera (Nikon DS-Ri1) mounted on an inverted fluorescence microscope (Ti−U, Nikon, Japan). A spinning-disk confocal microscope (Andor Revolution XD) was used to obtain confocal images. It was equipped with an Olympus IX 81 microscope, a Nipkow disk-type confocal unit (CSU 22, Yokogawa), and an EMCCD (Andor iXon DV885K) single photon detector. UV−vis absorption spectra were measured with a UV−vis spectrophotometer (UV-2550, Shimadzu Corporation). TEM images were obtained by a FEI Tecnai $G^2$ 20 TWIN electron microscope. Magnetic hysteresis loops were measured with a vibrating sample magnetometer (Lake Shore 7410 VSM). DLS measurements were performed on a Malvern Zetasizer Nano ZS instrument.

**Fabrication of Magnetic Nanospheres.** Magnetic nanospheres were fabricated according to our published LBL assembly method.[47] As illustrated in Scheme 1, Pst-AAm-COOH were prepared by an emulsifier-free polymerization method,[49,50] coated with a foundation layer of PEI (low MW 25 kDa), and then transferred into hexanol and incubated with hydrophobic nano-$\gamma$-$Fe_2O_3$. A second layer of PEI (high MW 750 kDa) was coated for attachment of an additional layer of nano-$\gamma$-$Fe_2O_3$. After five layers of nano-$\gamma$-$Fe_2O_3$ were assembled, an outer shell of silica was coated on the surface of the magnetic nanosphere with a seeded growth method. First, the magnetic nanospheres were transferred into ethanol containing 20 mg/mL PVP and incubated for 24 h with continuous stirring at room temperature. Then 90 $\mu$L of $NH_3$ (29.3 wt% in water) was added to the mixture, and immediately after that, 375 $\mu$L of TEOS (10 vol% in ethanol) was added in three steps under stirring over 24 h. After that, 125 $\mu$L of APTES (10 vol% in ethanol) was added and reacted for 12 h. The resultant amino-terminated silica-coated spheres were purified by magnetic separation with ethanol and dispersed in *N*,*N*-dimethylformamide (DMF) containing 0.01 g/mL succinic anhydride to react for 2 h. The final product, carboxyl-terminated magnetic nanospheres (MNs-COOH), was washed with ethanol three times and ultrapure water three times and kept in ultrapure water for use.

**Construction of Anti-EpCAM Antibody Modified Magnetic Nanospheres.** Carbodiimide chemistry was used to cross-link amines of the antibody with the carboxylic acid groups on the surface of MNs-COOH. Approximately 5 mg of MNs-COOH was activated in 50 mM EDC and 50 mM NHS in 1 mL of 0.01 M pH 6.8 PBS at room temperature with gentle shaking for 30 min. After that, the activated MNs-COOH were separated by a magnetic scaffold and washed with 0.01 M pH 7.2 PBS three times. Then, they were resuspended in 1 mL of 0.01 M pH 7.2 PBS to react with 50 $\mu$g of anti-EpCAM antibody for about 4 h with continuous shaking at room temperature. The resultant immunomagnetic nanospheres were washed with PBS to remove surplus antibody and then stored in 0.01 M pH 7.2 PBS at 4 °C for use.

**Capture of Spiked Tumor Cells in Buffer and Blood.** IMNs of different concentrations were used to capture SK-BR-3 cells ($1.0 \times 10^5$ cells per mL), and the numbers of cells captured and in the supernatant were all determined with a hemocytometer to calculate the corresponding capture efficiency. As controls, IMNs were used to treat Jurkat T cells and unmodified MNs were used to treat SK-BR-3 cells to investigate the specificity. Then, IMNs were used to capture rare tumor cells in synthetic CTC samples. Four groups of an extremely low concentration of SK-BR-3 cell-spiked samples were prepared as follows: Hoechst 33342-stained SK-BR-3 cells were spiked into 1× PBS, Jurkat T cell suspension ($10^6$ cells $mL^{-1}$ in 1× PBS), lysed blood, and whole blood with cell concentrations of approximately 5, 50, 100, 200, and 300 cells $mL^{-1}$. A certain amount of IMNs was added to the above samples to be incubated with gentle shaking at 37 °C. Then they were isolated and washed with a magnetic scaffold. The captured and uncaptured SK-BR-3 cells were all counted to calculate the capture efficiency. Additionally, IMNs and SK-BR-3 cells in whole blood were incubated for 5, 10, 20, and 30 min, respectively, to calculate the capture efficiency at different reaction times. Capture efficiencies from whole blood spiked with 100 cells of three other kinds of tumor cells (MCF-7, HuH-7, and Hep G2 cells) were also calculated to test the general applicability of this method. Whole blood samples were collected from healthy people into EDTA-coated vacutainer tubes and were used within 24 h.

**Capture and ICC Identification of Tumor Cells in Mimic Clinical Samples.** SK-BR-3 cells were spiked into healthy human whole blood with a concentration of approximately 50 cells $mL^{-1}$ to prepare closely mimicking clinical samples. Then IMNs were added to the samples, and the mixture was incubated for 5 min at 37 °C. After magnetic separation, the captured cells were fixed with 4% paraformaldehyde (10 min), permeabilized with 0.1% Triton-X 100 (10 min), blocked with 1% BSA (30 min), and stained with 30 $\mu$g/mL DAPI, FITC-labeled anti-CK19 monoclonal antibody, and APC-labeled anti-CD45 monoclonal antibody (30 min). After washing, the captured cells were put into a small PDMS device with a hole (diameter ~6 mm) stuck on the surface of a coverglass and attracted to the bottom by a magnet for confocal fluorescence microscopy imaging. Cells that had round to oval morphology and were positive for DAPI and CK19 and negative for CD45 were identified as tumor cells.

**Cell Viability Analyses.** A LIVE/DEAD viability kit was used to analyze the viability of the isolated cells. Briefly, the cells were stained with 2 $\mu$M calcein AM and 4.5 $\mu$M PI at room temperature for 30 min. Then the cells were observed under a fluorescence microscope excited with blue light, and 500 cells were counted to calculate the viability rate in triplicate. Further, SK-BR-3 cells captured with IMNs were cultured at 37 °C with Dulbecco's modified Eagle's medium (DMEM) containing 10% fetal bovine serum, 60 $\mu$g/mL penicillin G, and 100 $\mu$g/mL streptomycin sulfate in a humidified atmosphere with 5% $CO_2$. Sterile conditions should be maintained during the whole procedure.

**RT-PCR Assays.** Total RNA was extracted from cells using the RNAprep Pure Cell/Bacteria kit, and the RT reaction was performed with a Promega RT system according to the instructions. Then PCR assays of the SK-BR-3 cell complementary DNA (cDNA) were done by a Peltier thermal cycler (Bio-RAD). The specific primers of 5′-GACTACAGCCACTACTACACGACCAT-3′ and 5′-GAGCGGAATCCACCTCCACACT-3′ were used to amplify the 346-bp fragments of the human CK19 coding region, and the primers of 5′-CCAGTGACTGCTGCCACAACCA-3′ and 5′-CGCCGTCTTCCTCCATCTCATAGC-3′ were used to amplify the 285-bp fragments of the EGFR coding region. The PCR for CK19 followed the thermal profile 94 °C for 5 min, 35 cycles of 94 °C for 30 s, 55 °C for 30 s, 72 °C for 30 s, and a final extension at 72 °C for 10 min. For EGFR, the PCR thermal profile was 94 °C for 5 min, 35 cycles of 94 °C for 30 s, 67 °C for 30 s, 72 °C for 30 s, and a final extension at 72 °C for 10 min. The PCR products were separated in a 2% (wt/vol) agarose gel and stained with ethidium bromide for observation.

**Detection of CTCs in Cancer Patient Peripheral Blood Samples.** Blood samples from 19 cancer patients and 16 healthy normal controls were collected and treated with IMNs. Typically in each assay, a certain amount of blood was incubated with IMNs for 5 min. After enrichment, the isolated cells were identified with the three-color ICC and observed by a confocal fluorescence microscope, as described in the part ICC Identification of Tumor Cells in Mimic Clinical Samples. Only the cells with phenotypes of CK19 positive and DAPI positive but CD45 negative were enumerated as CTCs.

*Conflict of Interest:* The authors declare no competing financial interest.

*Acknowledgment.* This work was supported by the National Basic Research Program of China (973 Program, 2011CB933600), the 863 Program (2013AA032204), the Science Fund for Creative Research Groups of NSFC (20921062), the National Natural Science Foundation of China (21175100), the Program for New Century Excellent Talents in University (NCET-10-0656), the "3551 Talent Program" of the Administrative Committee of East Lake Hi-Tech Development Zone (Grant [2011]137), and the 111 Project (111-2-10). L.-L. Wu was supported by the Program for Cultivation of Inter-disciplinarily Innovative Talents of Wuhan University.

*Supporting Information Available:* S.1−S.7 (Figures S1−S6 and Tables S1 and S2). This material is available free of charge *via* the Internet at http://pubs.acs.org.

## REFERENCES AND NOTES


1. Fidler, I. J. The Pathogenesis of Cancer Metastasis: the 'Seed and Soil' Hypothesis Revisited. *Nat. Rev. Cancer* **2003**, *3*, 453–458.
2. Eccles, S. A.; Welch, D. R. Metastasis: Recent Discoveries and Novel Treatment Strategies. *Lancet* **2007**, *369*, 1742–1757.
3. Ring, A.; Smith, I. E.; Dowsett, M. Circulating Tumour cells in Breast Cancer. *Lancet Oncol.* **2004**, *5*, 79–88.
4. Arya, S. K.; Lim, B.; Rahman, A. R. A. Enrichment, Detection and Clinical Significance of Circulating Tumor Cells. *Lab Chip* **2013**, *13*, 1995–2027.
5. Cristofanilli, M.; Hayes, D. F.; Budd, G. T.; Ellis, M. J.; Stopeck, A.; Reuben, J. M.; Doyle, G. V.; Matera, J.; Allard, W. J.; Miller, M. C.; *et al*. Circulating Tumor Cells: A Novel Prognostic Factor for Newly Diagnosed Metastatic Breast Cancer. *J. Clin. Oncol.* **2005**, *23*, 1420–1430.
6. Ignatiadis, M.; Xenidis, N.; Perraki, M.; Apostolaki, S.; Politaki, E.; Kafousi, M.; Stathopoulos, E. N.; Stathopoulou, A.; Lianidou, E.; Chlouverakis, G.; *et al*. Different Prognostic Value of Cytokeratin-19 mRNA-Positive Circulating Tumor Cells According to Estrogen Receptor and HER2 Status in Early-Stage Breast Cancer. *J. Clin. Oncol.* **2007**, *25*, 5194–5202.
7. Cristofanilli, M.; Budd, G. T.; Ellis, M. J.; Stopeck, A.; Matera, J.; Miller, M. C.; Reuben, J. M.; Doyle, G. V.; Allard, W. J.; Terstappen, L. W. M. M.; *et al*. Circulating Tumor Cells, Disease Progression, and Survival in Metastatic Breast Cancer. *New Engl. J. Med.* **2004**, *351*, 781–791.
8. Wang, S. T.; Liu, K.; Liu, J.; Yu, Z. T. F.; Xu, X. W.; Zhao, L. B.; Lee, T.; Lee, E. K.; Reiss, J.; Lee, Y. K.; *et al*. Highly Efficient Capture of Circulating Tumor Cells by Using Nanostructured Silicon Substrates with Integrated Chaotic Micromixers. *Angew. Chem., Int. Ed.* **2011**, *50*, 3084–3088.
9. Pantel, K.; Brakenhoff, R. H.; Brandt, B. Detection, Clinical Relevance and Specific Biological Properties of Disseminating Tumour Cells. *Nat. Rev. Cancer* **2008**, *8*, 329–340.
10. Vona, G.; Sabile, A.; Louha, M.; Sitruk, V.; Romana, S.; Schütze, K.; Capron, F.; Franco, D.; Pazzagli, M.; Vekemans, M.; *et al*. Isolation by Size of Epithelial Tumor Cells: A New Method for the Immunomorphological and Molecular Characterization of Circulating Tumor Cells. *Am. J. Pathol.* **2000**, *156*, 57–63.
11. Hosokawa, M.; Hayata, T.; Fukuda, Y.; Arakaki, A.; Yoshino, T.; Tanaka, T.; Matsunaga, T. Size-Selective Microcavity Array for Rapid and Efficient Detection of Circulating Tumor Cells. *Anal. Chem.* **2010**, *82*, 6629–6635.
12. Huh, D.; Bahng, J. H.; Ling, Y.; Wei, H. H.; Kripfgans, O. D.; Fowlkes, J. B.; Grotberg, J. B.; Takayama, S. Gravity-Driven Microfluidic Particle Sorting Device with Hydrodynamic Separation Amplification. *Anal. Chem.* **2007**, *79*, 1369–1376.
13. He, W.; Kularatne, S. A.; Kalli, K. R.; Prendergast, F. G.; Amato, R. J.; Klee, G. G.; Hartmann, L. C.; Low, P. S. Quantitation of Circulating Tumor Cells in Blood Samples from Ovarian and Prostate Cancer Patients Using Tumor-Specific Fluorescent Ligands. *Int. J. Cancer* **2008**, *123*, 1968–1973.
14. Lim, L. S.; Hu, M.; Huang, M. C.; Cheong, W. C.; Gan, A. T. L.; Looi, X. L.; Leong, S. M.; Koay, E. S. W.; Li, M. H. Microsieve Lab-Chip Device for Rapid Enumeration and Fluorescence *in Situ* Hybridization of Circulating Tumor Cells. *Lab Chip* **2012**, *12*, 4388–4396.
15. Green, J. V.; Murthy, S. K. Microfluidic Enrichment of a Target Cell Type from a Heterogenous Suspension by Adhesion-Based Negative Selection. *Lab Chip* **2009**, *9*, 2245–2248.
16. Chen, W. Q.; Weng, S. N.; Zhang, F.; Allen, S.; Li, X.; Bao, L. W.; Lam, R. H. W.; Macoska, J. A.; Merajver, S. D.; Fu, J. P. Nanoroughened Surfaces for Efficient Capture of Circulating Tumor Cells without Using Capture Antibodies. *ACS Nano* **2013**, *7*, 566–575.
17. Nagrath, S.; Sequist, L. V.; Maheswaran, S.; Bell, D. W.; Irimia, D.; Ulkus, L.; Smith, M. R.; Kwak, E. L.; Digumarthy, S.; Muzikansky, A.; *et al*. Isolation of Rare Circulating Tumour Cells in Cancer Patients by Microchip Technology. *Nature* **2007**, *450*, 1235–1239.
18. Zhang, N. G.; Deng, Y. L.; Tai, Q. D.; Cheng, B. R.; Zhao, L. B.; Shen, Q. L.; He, R. X.; Hong, L. Y.; Liu, W.; Guo, S. S.; *et al*. Electrospun $TiO_2$ Nanofiber-Based Cell Capture Assay for Detecting Circulating Tumor Cells from Colorectal and Gastric Cancer Patients. *Adv. Mater.* **2012**, *24*, 2756–2760.
19. Plouffe, B. D.; Mahalanabis, M.; Lewis, L. H.; Klapperich, C. M.; Murthy, S. K. Clinically Relevant Microfluidic Magnetophoretic Isolation of Rare-Cell Populations for Diagnostic and Therapeutic Monitoring Applications. *Anal. Chem.* **2012**, *84*, 1336–1344.
20. Kang, J. H.; Krause, S.; Tobin, H.; Mammoto, A.; Kanapathipillai, M.; Ingber, D. E. A Combined Micromagnetic-Microfluidic Device for Rapid Capture and Culture of Rare Circulating Tumor Cells. *Lab Chip* **2012**, *12*, 2175–2181.
21. Myung, J. H.; Launiere, C. A.; Eddington, D. T.; Hong, S. Enhanced Tumor Cell Isolation by a Biomimetic Combination of E-Selectin and Anti-EpCAM: Implications for the Effective Separation of Circulating Tumor Cells (CTCs). *Langmuir* **2010**, *26*, 8589–8596.
22. Myung, J. H.; Gajjar, K. A.; Saric, J.; Eddington, D. T.; Hong, S. Dendrimer-Mediated Multivalent Binding for the Enhanced Capture of Tumor Cells. *Angew. Chem., Int. Ed.* **2011**, *123*, 11973–11976.
23. Sheng, W. A.; Chen, T.; Kamath, R.; Xiong, X. L.; Tan, W. H.; Fan, Z. H. Aptamer-Enabled Efficient Isolation of Cancer Cells from Whole Blood Using a Microfluidic Device. *Anal. Chem.* **2012**, *84*, 4199–4206.
24. Bamrungsap, S.; Chen, T.; Shukoor, M. I.; Chen, Z.; Sefah, K.; Chen, Y.; Tan, W. H. Pattern Recognition of Cancer Cells Using Aptamer-Conjugated Magnetic Nanoparticles. *ACS Nano* **2012**, *6*, 3974–3981.
25. Cremoux, P.; Extra, J. M.; Denis, M. G.; Pierga, J. Y.; Bourstyn, E.; Nos, C.; Clough, K. B.; Boudou, E.; Martin, E. C.; Müller, A.; *et al*. Detection of MUC1-Expressing Mammary Carcinoma Cells in the Peripheral Blood of Breast Cancer Patients by Real-Time Polymerase Chain Reaction. *Clin. Cancer Res.* **2000**, *6*, 3117–3122.
26. Galanzha, E. I.; Shashkov, E. V.; Kelly, T.; Kim, J. W.; Yang, L.; Zharov, V. P. *In Vivo* Magnetic Enrichment and Multiplex Photoacoustic Detection of Circulating Tumour Cells. *Nat. Nanotechnol.* **2009**, *4*, 855–860.
27. Xu, H. Y.; Aguilar, Z. P.; Yang, L.; Kuang, M.; Duan, H. W.; Xiong, Y. H.; Wei, H.; Wang, A. Antibody Conjugated Magnetic Iron Oxide Nanoparticles for Cancer Cell Separation in Fresh Whole Blood. *Biomaterials* **2011**, *32*, 9758–9765.
28. Witzig, T. E.; Bossy, B.; Kimlinger, T.; Roche, P. C.; Ingle, J. N.; Grant, C.; Donohue, J.; Suman, V. J.; Harrington, D.; Torre-Bueno, J.; *et al*. Detection of Circulating Cytokeratin-Positive Cells in the Blood of Breast Cancer Patients Using Immunomagnetic Enrichment and Digital Microscopy. *Clin. Cancer Res.* **2002**, *8*, 1085–1091.
29. Talasaz, A. H.; Powell, A. A.; Huber, D. E.; Berbee, J. G.; Roh, K. H.; Yu, W.; Xiao, W. Z.; Davis, M. M.; Pease, R. F.; Mindrinos, M. N.; *et al*. Isolating Highly Enriched Populations of Circulating Epithelial Cells and Other Rare Cells from Blood Using a Magnetic Sweeper Device. *Proc. Natl. Acad. Sci. U. S.A.* **2009**, *106*, 3970–3975.
30. Riethdorf, S.; Fritsche, H.; Müller, V.; Rau, T.; Schindlbeck, C.; Rack, B.; Janni, W.; Coith, C.; Beck, K.; Jänicke, F.; *et al*. Detection of Circulating Tumor Cells in Peripheral Blood of Patients with Metastatic Breast Cancer: A Validation Study of the CellSearch System. *Clin. Cancer Res.* **2007**, *13*, 920–928.
31. Zhong, X. Y.; Kaul, S.; Lin, Y. S.; Eichler, A.; Bastert, G. Sensitive Detection of Micrometastases in Bone Marrow from Patients with Breast Cancer Using Immunomagnetic Isolation of Tumor Cells in Combination with Reverse Transcriptase/Polymerase Chain Reaction for Cytokeratin-19. *J. Cancer Res. Clin. Oncol.* **2000**, *126*, 212–218.

32. Flatmark, K.; Bjørnland, K.; Johannessen, H. O.; Hegstad, E.; Rosales, R.; Hårklau, L.; Solhaug, J. H.; Faye, R. S.; Søreide, O.; Fodstad, Ø. Immunomagnetic Detection of Micrometastatic Cells in Bone Marrow of Colorectal Cancer Patients. *Clin. Cancer Res.* **2002**, *8*, 444–449.
33. Tong, X. D.; Yang, L. Y.; Lang, J. C.; Zborowski, M.; Chalmers, J. J. Application of Immunomagnetic Cell Enrichment in Combination with RT-PCR for the Detection of Rare Circulating Head and Neck Tumor Cells in Human Peripheral Blood. *Cytometry, Part B* **2007**, *72*, 310–323.
34. Yavuz, C. T.; Mayo, J. T.; Yu, W. W.; Prakash, A.; Falkner, J. C.; Yean, S.; Cong, L.; Shipley, H. J.; Kan, A.; Tomson, M.; *et al.* Low-Field Magnetic Separation of Monodisperse $Fe_3O_4$ Nanocrystals. *Science* **2006**, *314*, 964–967.
35. Zhao, W.; Zhang, W. P.; Zhang, Z. L.; He, R. L.; Lin, Y.; Xie, M.; Wang, H. Z.; Pang, D. W. Robust and Highly Sensitive Fluorescence Approach for Point-of-Care Virus Detection Based on Immunomagnetic Separation. *Anal. Chem.* **2012**, *84*, 2358–2365.
36. Wen, C. Y.; Hu, J.; Zhang, Z. L.; Tian, Z. Q.; Ou, G. P.; Liao, Y. L.; Li, Y.; Xie, M.; Sun, Z. Y.; Pang, D. W. One-Step Sensitive Detection of *Salmonella typhimurium* by Coupling Magnetic Capture and Fluorescence Identification with Functional Nanospheres. *Anal. Chem.* **2013**, *85*, 1223–1230.
37. An Introduction to the CellSearch System.
38. Wang, G. P.; Song, E. Q.; Xie, H. Y.; Zhang, Z. L.; Tian, Z. Q.; Zuo, C.; Pang, D. W.; Wu, D. C.; Shi, Y. B. Biofunctionalization of Fluorescent-Magnetic-Bifunctional Nanospheres and Their Applications. *Chem. Commun.* **2005**, 4276–4278.
39. Song, E. Q.; Wang, G. P.; Xie, H. Y.; Zhang, Z. L.; Hu, J.; Peng, J.; Wu, D. C.; Shi, Y. B.; Pang, D. W. Visual Recognition and Efficient Isolation of Apoptotic Cells with Fluorescent-Magnetic-Biotargeting Multifunctional Nanospheres. *Clin. Chem.* **2007**, *53*, 2177–2185.
40. Xie, M.; Hu, J.; Long, Y. M.; Zhang, Z. L.; Xie, H. Y.; Pang, D. W. Lectin-Modified Trifunctional Nanobiosensors for Mapping Cell Surface Glycoconjugates. *Biosens. Bioelectron.* **2009**, *24*, 1311–1317.
41. Song, E. Q.; Hu, J.; Wen, C. Y.; Tian, Z. Q.; Yu, X.; Zhang, Z. L.; Shi, Y. B.; Pang, D. W. Fluorescent-Magnetic-Biotargeting Multifunctional Nanobioprobes for Detecting and Isolating Multiple Types of Tumor Cells. *ACS Nano* **2011**, *5*, 761–770.
42. Hu, J.; Xie, M.; Wen, C. Y.; Zhang, Z. L.; Xie, H. Y.; Liu, A. A.; Chen, Y. Y.; Zhou, S. M.; Pang, D. W. A Multicomponent Recognition and Separation System Established *via* Fluorescent, Magnetic, Dualencoded Multifunctional Bioprobes. *Biomaterials* **2011**, *32*, 1177–1184.
43. Li, Y. Y.; Zhou, Y. L.; Wang, H. Y.; Perrett, S.; Zhao, Y. L.; Tang, Z. Y.; Nie, G. J. Chirality of Glutathione Surface Coating Affects the Cytotoxicity of Quantum Dots. *Angew. Chem., Int. Ed.* **2011**, *50*, 5860–5864.
44. Liu, X. F.; Zhang, L.; Zeng, J.; Gao, Y.; Tang, Z. Y. Superparamagnetic Nano-Immunobeads toward Food Safety Insurance. *J. Nanopart. Res.* **2013**, *15*, 1796–1806.
45. Qin, B.; Chen, H. Y.; Liang, H.; Fu, L.; Liu, X. F.; Qiu, X. H.; Liu, S. Q.; Song, R.; Tang, Z. Y. Reversible Photoswitchable Fluorescence in Thin Films of Inorganic Nanoparticle and Polyoxometalate Assemblies. *J. Am. Chem. Soc.* **2010**, *132*, 2886–2888.
46. Li, X. Y.; Zhou, Y. L.; Zheng, Z. Z.; Yue, X. L.; Dai, Z. F.; Liu, S. Q.; Tang, Z. Y. Glucose Biosensor Based on Nanocomposite Films of CdTe Quantum Dots and Glucose Oxidase. *Langmuir* **2009**, *25*, 6580–6586.
47. Xie, M.; Hu, J.; Wen, C. Y.; Zhang, Z. L.; Xie, H. Y.; Pang, D. W. Fluorescent-Magnetic Dual-Encoded Nanospheres: A Promising Tool for Fast-Simultaneous-Addressable High-Throughput Analysis. *Nanotechnology* **2012**, *23*, 035602.
48. Weigelt, B.; Peterse, J. L.; Veer, L. J. V. Breast Cancer Metastasis: Makers and Models. *Nature* **2005**, *5*, 591–602.
49. Xie, H. Y.; Zuo, C.; Liu, Y.; Zhang, Z. L.; Pang, D. W.; Li, X. L.; Gong, J. P.; Dickinson, C.; Zhou, W. Z. Cell-Targeting Multifunctional Nanospheres with Both Fluorescence and Magnetism. *Small* **2005**, *1*, 506–509.
50. Xie, H. Y.; Xie, M.; Zhang, Z. L.; Long, Y. M.; Liu, X.; Tang, M. L.; Pang, D. W.; Tan, Z.; Dickinson, C.; Zhou, W. Z. Wheat Germ Agglutinin-Modified Trifunctional Nanospheres for Cell Recognition. *Bioconjugate Chem.* **2007**, *18*, 1749–1755.